

# Biaxial Testing Machine for Mixed Mode Cracking of Concrete

L. Østergaard, J.F. Olesen & P.N. Poulsen

*Department of Civil Engineering, Technical University of Denmark, 2800 Kgs. Lyngby*

**ABSTRACT:** Cracks in concrete may open in two fundamentally different modes in plane problems; normal to the crack plane (Mode I) and sliding of the crack faces (Mode II). A general loading situation consisting of an arbitrary combination of normal and shear stresses will invoke a combination of the two fundamental opening modes, i.e. leading to mixed mode cracking. Detailed experimental knowledge of the initiation and propagation of cracks in concrete under mixed mode loading is an important prerequisite for the formulation of mixed mode fracture mechanical models. For this purpose, an extremely stiff, bi-axial testing machine with mutually independent servo-hydraulic pumps has been developed. The setup is designed with non-rotating boundary platens, and the rotational stiffness has been measured to approximately 8000 kNm/rad. The crack initiation and crack propagation is measured locally on the surface of the specimen by photogrammetric techniques. The sample experiments presented cover both notched and un-notched specimens. The un-notched specimens were designed to study crack initiation, and it appears that cracks initiate purely in Mode I, while Mode II sliding displacements only grow slowly in magnitude. The notched specimens revealed that it is difficult to conduct mixed mode experiments for small crack widths since new cracks tend to initiate and since the crack may not necessarily have propagated all the way through the specimen.

## 1 INTRODUCTION

The proper modelling of fracture processes in concrete structures involves mixed mode conditions. Here we refer to mixed mode fracture when the crack opening involves both Mode I and Mode II deformations. Further, we assume that stresses act on the crack faces once they have been established: Cohesive stresses normal to the crack face, and shear stresses tangential to the crack face. Once the crack has been formed (presumably in Mode I, i.e. perpendicular to the first principle stress direction) it may, at later stages of loading, be subject to mixed mode conditions. The mixed mode situation will give rise to dilation and possibly the build up of normal compressive stresses and consequently increase shear stresses. This mixed mode fracture model may be seen as an extended fictitious crack model, and in principle it lends itself easily to a numerical implementation e.g. in the framework of the eXtended Finite Element Method (XFEM). However, the constitutive relationship for the crack, i.e. the relationships between the normal and tangential stresses and the normal and tangential deformations are complex and not one-to-one, since they are bound to be functions of the load and deformation histories. This implies an incremen-

tal approach to the modelling, and efforts have been made to establish the incremental constitutive relationship for mixed mode crack behaviour in concrete, see e.g. Carol et al. (2001) in which an approach based in non-associated plasticity and damage mechanics is demonstrated.

Experimental investigations on mixed mode fracture of concrete have been the topic of a number of publications since Hillerborg et al. (1976) published their paper on the fictitious crack model. Most of the publications deal with the four point shear beam (FPSB) or similar, structural experiments, in order to promote mixed-mode crack propagation, see e.g. the work by Carpinteri and Swartz (1991) and Gálvez et al. (1998), where comprehensive reference lists are given. The problem with such tests is that it is almost impossible to enforce a uniform and specific state of mixed mode opening of the crack planes. Focusing on contributions using a dedicated biaxial testing machine, only two major publications are available: The ph.d.-theses by Hassanzadeh (1992) and Nooru-Muhamed (1992). The experimental setups developed in these research projects are shown in Figure 1 and 2. Nooru-Muhamed (1992) developed a setup in which three frames were used to induce the mixed mode loading conditions. The inner frame moves vertically

and is attached to the top of the specimen, while the outer frames are coupled and move horizontally, being attached to the bottom of the specimen. Hassanzadeh (1992) developed a setup suited for being built into a standard testing machine which imposes the normal opening of the crack. A special arrangement (see Figure 2) employing a horizontal actuator, is used for applying the shear load.

These setups have been used to generate a large number of experimental results for many different opening modes of the crack. However, a number of issues remain unclear or unresolved following their work. First of all, the stiffness of the setups are unclear and in the work by Hassanzadeh (1992), comments are made that the setup was not sufficiently stiff. This resulted in a hump on the unloading branch, which is normally associated with insufficient stiffness, see e.g. Hillerborg (1989). Another issue which is unclear is whether the crack has actually propagated all the way through the specimens when the mixed mode loading conditions are imposed. Initially, Hassanzadeh (1992) opens the crack in Mode I and assumes that immediately after unloading has commenced, the crack has propagated all the way through the specimen. This assumption needs verification. It is also unclear whether the crack propagation is localized in one single crack for all combinations of mixed mode loading, or whether at some point, with a certain degree of crack sliding, either secondary cracks initiate, or a non-local, compressive failure occurs. Finally, it is of interest to know whether the crack may initiate in Mode II at all.

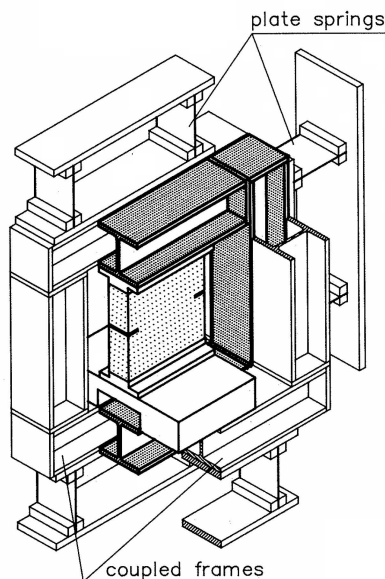


Figure 1: Biaxial testing machine by Nooru-Muhamed (1992). The inner frame moves vertically while the two coupled outer frames move horizontally. The top of the specimen is attached to the inner frame and the bottom to the outer frames.

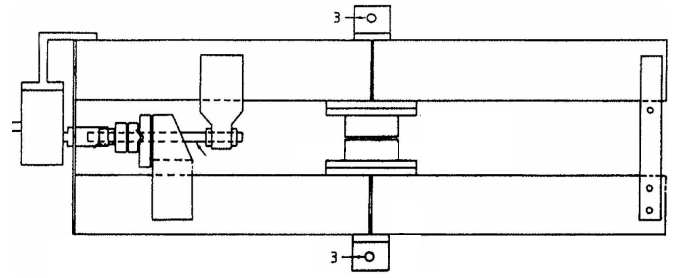


Figure 2: Biaxial testing machine by Hassanzadeh (1992). Normal load is imposed using a testing machine attached to the holes placed above and below the centrally placed specimen, while shear loading is applied using the horizontal actuator shown to the left.

This work focuses on presentation of the ideas behind the development of a biaxial testing machine that is sufficiently stiff for the conduction of rotationally and translational stable fracture mechanical experiments. After documenting these features, experiments with the focus of studying crack initiation modes, crack localization conditions, and the point of full crack penetration in the uniaxial tension test (UTT), will be presented. The results represent pilot tests with the biaxial setup, and more results will be presented in the future. This work is carried out in collaboration with the fracture mechanics group at the Technical University of Denmark.

## 2 CONCEPTS OF THE SETUP

The concepts of the present biaxial testing machine are shown in Figure 3. The idea is to build a machine which can impose simultaneously and independently normal- and shear loads on a concrete specimen. This is achieved by using two independent actuators, controlled by multi-axial Instron 8500+ hardware and modified LabView-based Instron subroutines. The setup is built into a four column Instron 5MN universal testing machine giving a very stiff and full functional vertical axis of loading. The horizontal axis is designed specially for the purpose at hand using an ESH actuator built onto a very stiff support structure such that the shear load is carried from the actuator through the specimen and back to the actuator through compression in the support structure.

A special detail, emphasized in Figure 3 is the linear motion (LM) system. These LM blocks and rails are high-precision machined elements usually applied in automatized production and robotics. The detail in Figure 3 shows how the LM system is capable of carrying both compressive and tensile loads through the four raceways with ball bearings. Each raceway is a closed circuit and the balls may travel from the loaded part into an unloaded channel within the LM block and back to the load bearing part depending on the

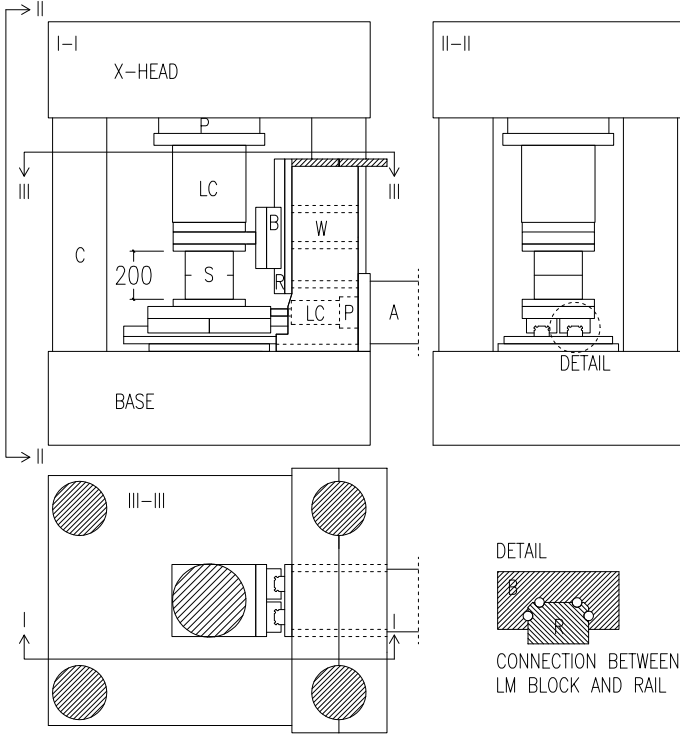


Figure 3: Present the biaxial setup, A = actuator, P = piston, LC = load cell, S = specimen, C = column, B = linear motion block (LM block), R = Rail, W = web. Details in the background left out for clarity.

movements imposed on the system.

The bolted connections in the setup are all pre-stressed such that no slip between the platens will occur during the experiment. Finally, it is noted that the specimen is glued into the setup using sandblasted steel platens. This connection gives the most uniform transfer of stresses and an easy insertion and removal of the individual specimens.

The setup has initially been designed for specimens with a cross section of up to 200 x 200 mm<sup>2</sup>. However, in practice, the maximum specimen size must be determined on the basis of stability considerations concerning the crack propagation, using the actually obtained rotational and translational stiffness of the setup. This is the topic of the next section.

### 3 DESIGN CONSIDERATIONS

According to Petersson (1981) and Hillerborg (1989) translational and rotational stability of crack propagation in Mode I fracture experiments is achieved if the following conditions are fulfilled:

$$S_t = A \left( -\frac{d\sigma}{dw} \right) \left( \frac{1}{K_{m,t}} + \frac{1}{K_{s,t}} \right) < 1 \quad (1)$$

$$S_r = I \left( -\frac{d\sigma}{dw} \right) \left( \frac{1}{K_{m,r}} + \frac{1}{K_{s,r}} \right) < 1 \quad (2)$$

in which  $A$  is the area and  $I$  is the moment of inertia of the notched part of the specimen. The max-

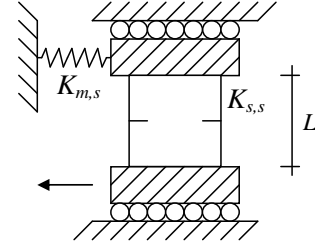


Figure 4: Simplified system used for the calculation of condition for shear stability of fracture testing. The support structure is designed such that it is far more stiff than the shear stiffness of the vertical actuator, and thus, the latter has been omitted from the analysis.

imum slope of the  $\sigma$ - $w$  relationship is denoted by  $d\sigma/dw$ , while  $K_{m,t}$  and  $K_{m,r}$  are the rotational and the translational stiffness of the machine. The corresponding translational and rotational stiffness of the specimen are denoted  $K_{s,t}$  and  $K_{s,r}$ , respectively. The measured values of  $K_{m,r}$  and  $K_{m,t}$  for the biaxial testing machine described in this study are approximately  $K_{m,r} = 8000$  kNm/rad and  $K_{m,t} = 500$  kN/mm. The values were measured on two perpendicular horizontal axes and the lowest values are reported here. Note that the values are much higher than reported elsewhere in literature, see e.g. Hordjik (1991), who measured  $K_{m,r} = 1000$  kNm/rad. Note also, that the condition in Equation (1) is only relevant if the experiment is stroke controlled - closed loop controlled experiments do not share this requirement since the measuring length is normally considerably smaller. Also stability of crack propagation in Mode II fracture must be achieved. An expression similar to Equations (1) and (2), assuming a simplified system as shown in Figure 4, can be derived and the result is:

$$S_s = A \left( -\frac{d\tau}{dv} \right) \left( \frac{1}{K_{m,s}} + \frac{L}{K_{s,s}} \right) < 1 \quad (3)$$

in which  $d\tau/dv$  is the steepest slope of a theoretical Mode II  $\tau$ - $v$  crack sliding relationship,  $K_{m,s}$  is the stiffness of the testing machine when the specimen is loaded in shear,  $K_{s,s}$  is the shear stiffness of the specimen and  $L$  is the length of the specimen. However, the steepest slope of this  $\tau$ - $v$  relationship is not known, and thus, the design criterium in Equation (3) has not been verified a priori. Regarding the translational and rotational stabilities, Equations (1) and (2) have been applied to determine an appropriate specimen size given the measured rotational and translational stiffness of the machine. Based on these expressions a specimen size with a height of  $h = 150$  mm, width of  $b = 150$  mm and thickness of  $t = 100$  mm has been chosen. If the reduction of the specimen stiffness due to the presence of the notch is disregarded, these dimensions give  $S_t = 0.66$  and  $S_r = 0.04$  for a concrete with the assumed parameters  $E = 30$  GPa and

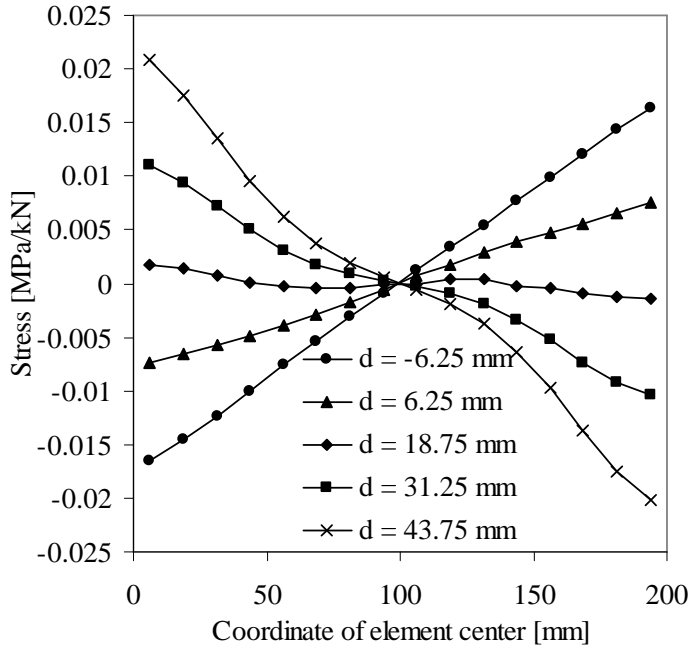


Figure 5: Normal stress distribution caused by shear load for different sections close to center of specimen (center is located at  $d = 0$  mm).

$$d\sigma/dw = 40 \text{ MPa/mm.}$$

Another key design criterium has been to ensure that the normal stresses in the notched section of the specimen, where the crack will initiate and propagate, are as uniform as possible, i.e. that the moment is zero in this section. It is expected that this will be the situation near the center of the specimen since the modulus of elasticity of the concrete is much lower than that of the other parts of the setup. However, this has been tested in a linear elastic finite element model simulating realistic boundary conditions of the machine, i.e. using elastic layers with properties corresponding to those of the rails, the LM blocks, the vertical testing machine etc. The result is illustrated in Figure 5. The specimen modelled is without a notch,  $b = 200$  mm wide and  $L = 200$  mm long, and a total of  $16 \times 16$  elements were used for the specimen. Thus, the element dimensions were  $12.5 \times 12.5 \text{ mm}^2$ . The stresses given in the figure represent the mean stress in each element. The modulus of elasticity for the concrete was  $E = 30 \text{ GPa}$  and the shear loading was  $V = 1 \text{ kN}$ . The result is that the moment is close to zero in the element row where the element centers are placed  $18.75 \text{ mm}$  away from the specimen centerline. Further analysis into this issue has shown that the section with zero moment approaches the specimen center for low values of  $E$ , while the neutral section stays within a distance of  $d = 25 \text{ mm}$  for  $E < 80 \text{ GPa}$ . Thus, for any type of concrete, the notch can be cut at the specimen center without introducing any significant error due to moment.

A number of other design considerations will shortly be described. The linear motion blocks (LM blocks) were selected for highest possible rigidity.

Besides the particular design of the chosen model, this is achieved by selecting steel balls with a slight oversize. Thus, upon assembly, a certain prestress is present, and the system has a high stiffness from un-set of tensile loading. However, due to this fact, together with the viscosity resistance of the lubricant and the load exerted on the system, a small fraction of the horizontal and vertical load will go through the rails, rather than through the specimen. On the other hand, since high precision linear motion guides with ball bearings have been used, the coefficient of friction is in the order of  $0.002 - 0.003$ , and thus, this loss of load is insignificant. See also the product catalog, THK (2000).

The design load for shear force has been determined on basis of the theoretical pure Mode II experiment with suppressed dilation. In this situation, assuming a ligament size of  $200 \times 100 \text{ mm}^2$ , the maximum shear loading is calculated on basis of a model concrete with  $f_c = 50 \text{ MPa}$ , i.e.  $V = f_c b t / 4 = 250 \text{ kN}$ . In the case of the normal load, the limiting case has been the pure uniaxial compression test for a specimen size of  $100 \times 100 \text{ mm}^2$ , i.e.  $N = f_c b t = 500 \text{ kN}$ .

Another issue which must be quantified concerns the absorption of transverse loads and moments by the horizontal and vertical load cell and actuator. It is clear that in the ideal situation, only a longitudinal force is exerted on these components since, otherwise, measurement errors and damage to the components may occur. The transverse loads and moments have been minimized by measuring the shear stiffness of the individual components and designing a system whose rigidity is so high that only a tiny fraction of the transverse loads are absorbed in the load cells and actuators. This is one of the reasons for the large dimensions of the support structure seen in Figure 3. Through the finite element model it has been documented that only a few percent of the shear load from the horizontal actuator is absorbed by the vertical actuator (about  $5 \text{ kN}$  for a shear load of  $250 \text{ kN}$ ) for the system built. This fraction is even smaller for the shear load absorbed by the horizontal load cell from the vertical load since the normal stiffness of the setup is extremely high compared with the stiffness of the load cell and steel bar which connects the horizontal actuator to the system.

#### 4 MEASUREMENT TECHNIQUES

For measuring of the crack openings a photogrammetric equipment has been used. The system, Aramis, manufactured by GOM mbh, uses digital stereo photographing and subsequent triangulation to determine 3D displacements on the surface of the specimen. The surface needs to be prepared with black dots of a certain size, preferably arranged in a speckle pattern,



Figure 6: Biaxial testing machine shown together with the Aramis cameras in the foreground. The horizontal actuator is seen to the left.

painted on a white background. Analysis is carried out by dedicated software which analyzes the movement and deformation of so-called facets, i.e. small sections of the surface, typically  $15 \times 15$  pixels of the digital image. The resolution of the equipment in terms of deformation is normally  $10^{-5}a$ , where  $a$  is the side length of the measuring area. Thus, if  $a = 100$  mm, the resolution is of the order of  $1 \mu\text{m}$ . The corresponding strain resolution is in the range of  $100 \mu\epsilon$  and thus, the equipment is not sufficiently sensitive for measuring concrete elastic strains, e.g. in front of the crack tip. The equipment is very flexible and may be used for laboratory specimens of almost any size. The application of the Aramis setup together with the biaxial testing machine is shown in Figure 6. Figure 7 shows a close view of the biaxial testing machine with a notched specimen inserted.

## 5 EXPERIMENTAL RESULTS & DISCUSSION

Figures 8 - 11 show different stages during an experiment for a specimen loaded in shear with suppressed normal displacement, i.e.  $W \equiv 0$ ,  $V = V(t)$ , where  $W$  and  $V$  are the remote normal and shear displacements (position of vertical and horizontal actuator).

The figures show the dogbone shaped specimen with a semitransparent overlay depicting the major strain calculated by Aramis. Aramis has been setup such that the strain illustration color is bright when the major strain is below 0.2% and dark above this value. Note that the usage of strain is only for visualization purposes since the definition of strain makes no sense in combination with localized cracking. The normal and shear loads corresponding to each pic-

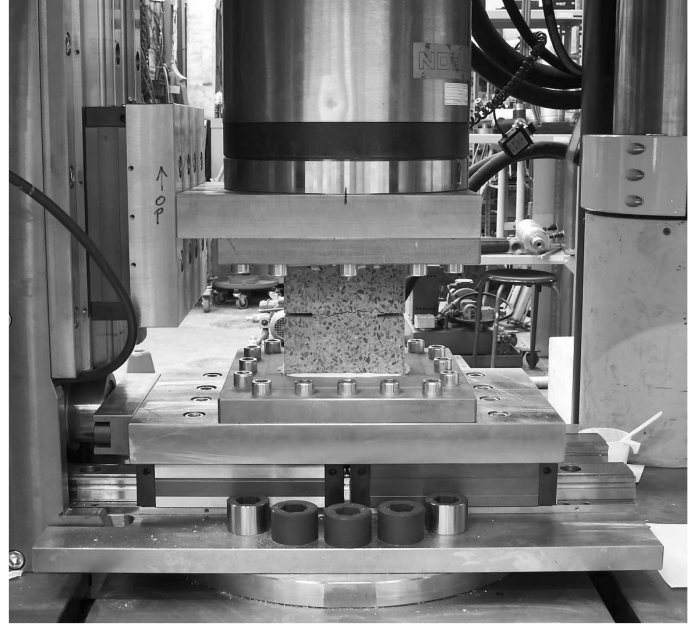


Figure 7: Close view of the biaxial testing machine.

ture are shown in Figure 12 using upward triangles. The first crack at the boundary is expected due to the load concentration caused by the geometry. However, it is the crack in the center of the specimen which is interesting since the crack here is free to initialize either in Mode I, Mode II or any combination thereof, and thus, this crack has undergone detailed analysis. One of the advantages using Aramis is that virtual clip gages can be placed at relevant positions on the specimen in the post processing phase. Therefore, in Figure 13, the results from two such measurements are given; one, which passes the center crack, and one with same gage length and orientation however placed in the uncracked material neighboring this crack. The two measurements are given together with a curve showing the pure crack opening and sliding, calculated by subtracting the two aforementioned virtual clip gage measurements. The slope of the  $\Delta_{cr}$ -curve is initially very low, the result of a linear regression is 0.003 in the range  $0 < w < 0.05$  mm, i.e. the crack initiates in pure Mode I. This is also the observation obtained from a number of other experiments with crack initiation away from the specimen boundary. However, at a certain crack opening,  $w_{min} \cong 0.05$  mm, mode II opening of the crack initiates. It is noticeable that the calculated  $\Delta_{cr}$ -curve does not originate in  $(w, v) = (0, 0)$  as expected. However, the reason for the small discrepancy, approximately 0.005 mm, is the fact that the deformations are measured on two different parts of the specimen, i.e. over the crack and neighboring the crack.

Based on Figure 12, the stresses of the center section of the specimen, i.e. at the location where the center crack initiates, have been estimated using simple linear elastic formulas. The normal stress,  $\sigma = N/tb$  and the shear stress,  $\tau = 3/2 \cdot V/tb$  were used to cal-

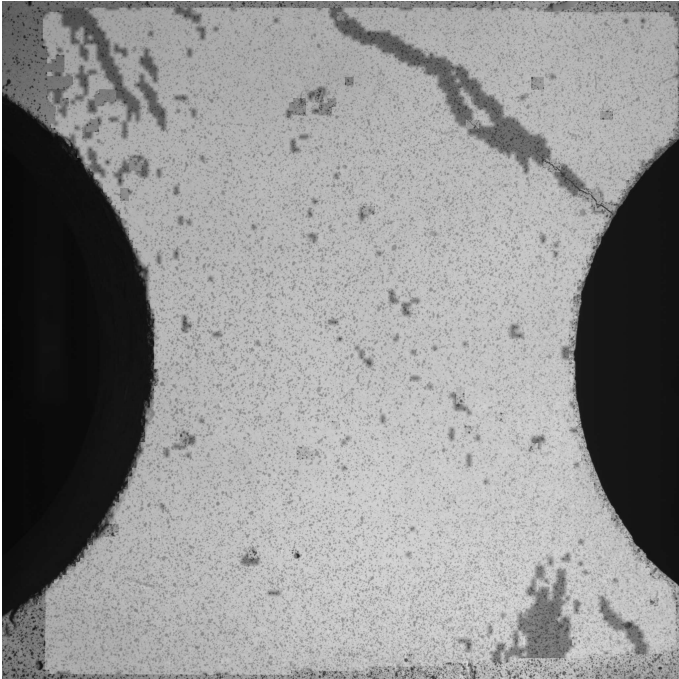


Figure 8: Shear-loaded specimen after initialization of first crack.

culate the value and direction of the principal stresses. The principal stresses were  $\sigma_1 = 4.4$  MPa and  $\sigma_2 = -11.6$  MPa and the direction  $\theta = 58^\circ$  where  $\theta = 0^\circ$  is the horizontal direction. Whereas the magnitude of  $\sigma_1$  seems to exceed the tensile strength of the material, the actual direction of the center crack seen on Figure 9 is  $\theta = 52^\circ$  and thus almost coinciding with the estimate. It is noted that the first principal stress is higher than the expected tensile strength. Probable reasons include the crude estimate of the stresses in the cross section analyzed, of fewer and smaller defects in the

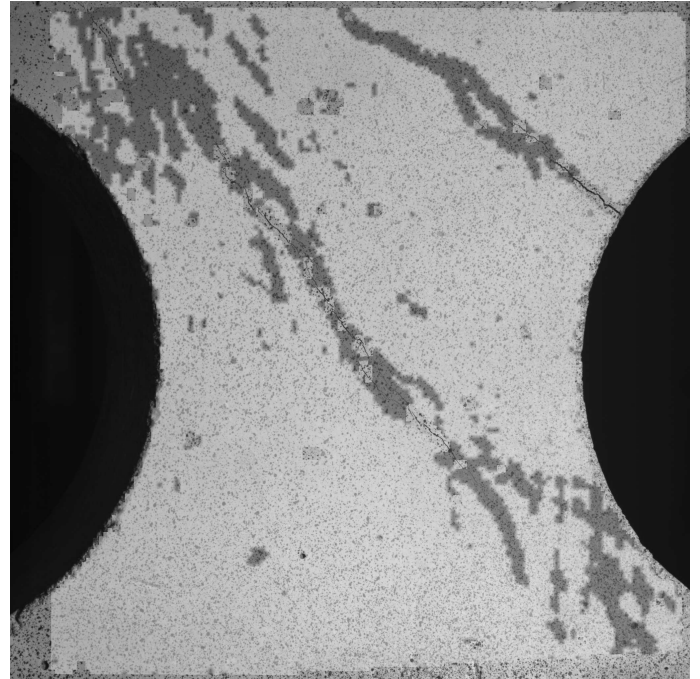


Figure 10: Shear-loaded specimen after opening of second crack.

center of the specimen.

The pilot tests on the DTU biaxial testing machine did also include uniaxial tension tests (UTT). These were conducted to see at which point the crack has fully penetrated the specimen. The specimens in this study were noticed by a sawcut resembling the typical UTT specimen preparation, see e.g. RILEM (2001) or Figures 7 and 14. The result is that it appears that there is no definitive point on the load-CMOD curve at which the crack has fully penetrated the specimen.

For some experiments, a uniformly opened crack

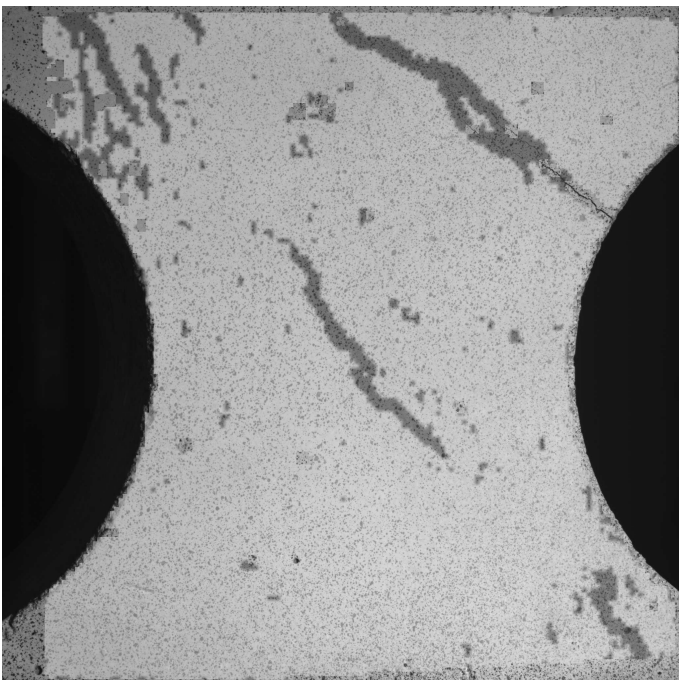


Figure 9: Shear-loaded specimen after initialization of second crack in center.

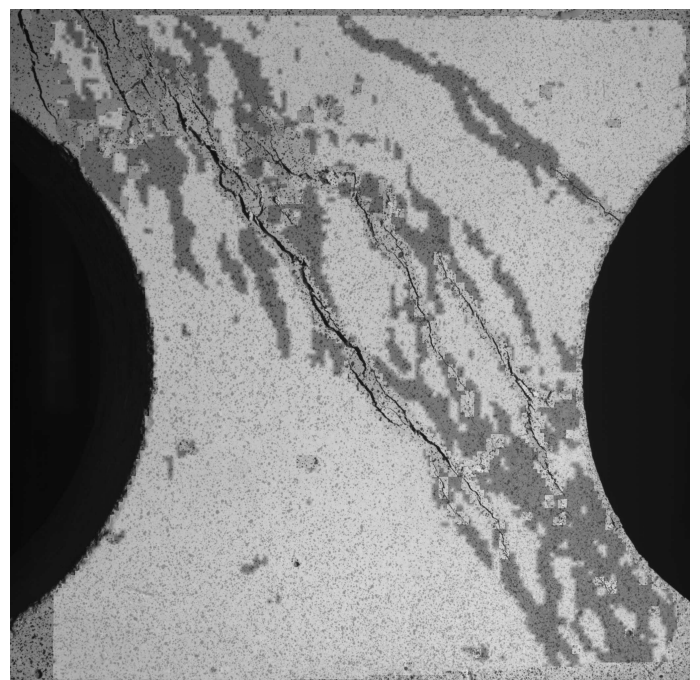


Figure 11: Shear-loaded specimen in a late stage with multiple cracks.

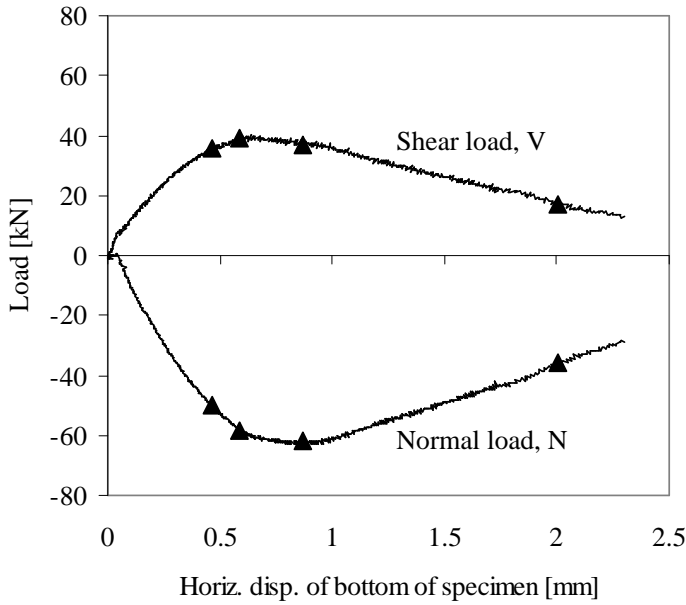


Figure 12: Horizontal displacement of specimen vs. shear,  $V$ , and normal,  $N$ , load on the specimen. The triangles refer to the pictures in Figures 8-11.

is established throughout the specimen right after the peak load while other results show that this situation is not obtained until the load has decreased to 50 – 80% of the peak load. In fact, most of the experiments show the latter behavior and thus, it is difficult to establish an experiment in which mixed-mode models may be verified for small crack widths.

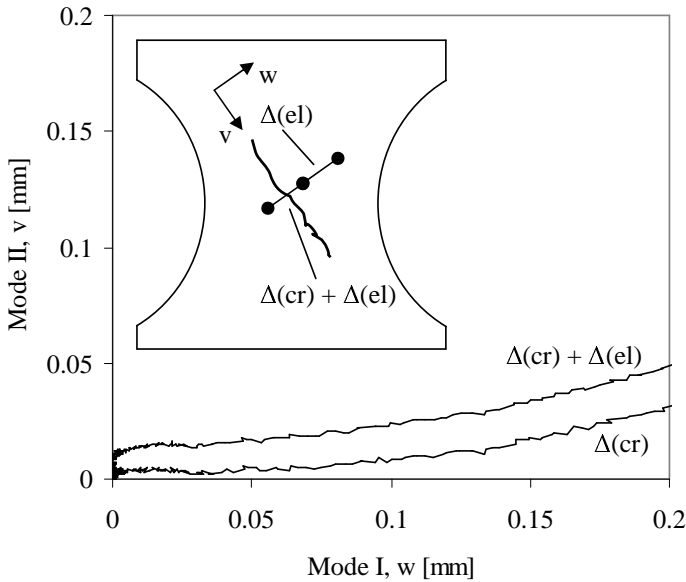


Figure 13: Crack initialization mode in center of specimen. The remote boundary conditions were: suppressed normal displacement,  $W \equiv 0$  and constant rate of shear displacement,  $V = V(t)$ . Virtual clip gages were used to measure the displacements over the crack,  $\Delta_{cr} + \Delta_{el}$ , and the displacements on a section outside the crack,  $\Delta_{el}$ . These results were used to calculate the inelastic displacements,  $\Delta_{cr}$ . Normal opening is denoted by  $w$  while crack sliding is denoted by  $v$ . The gage lengths are exaggerated for the purpose of illustration.

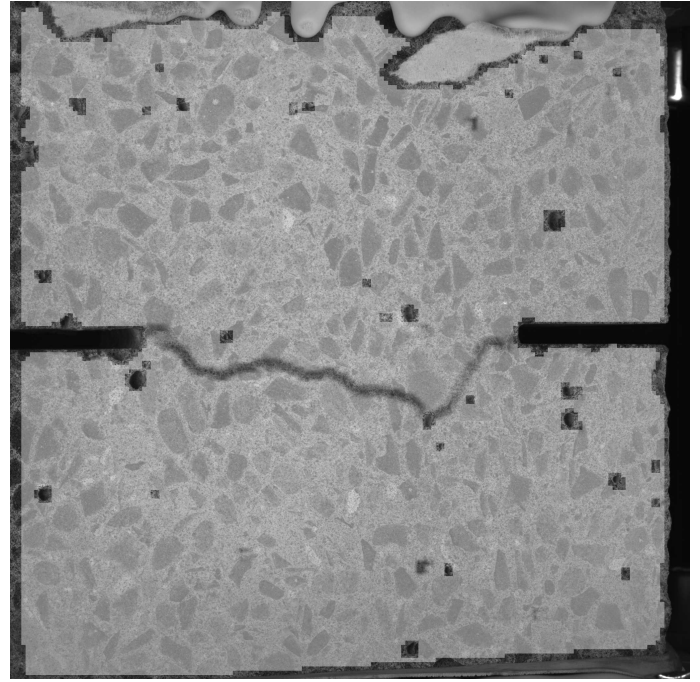


Figure 14: Primary crack established in uniaxial tension. The load has dropped to approx. 50% of peak load in the situation shown.

Mixed-mode experiments were also carried out in the pilot phase. The idea was to test mixed-mode opening of cracks, already established in mode I. Due to the uncertainty concerning the point of full crack penetration, shear loading of the specimen was not initiated until the normal load had decreased to approximately 50%. For easy reference to the individual experiments, the mixed-mode angle  $\varphi$  is defined. For a pure UTT ( $V \equiv 0, W = W(t)$ ),  $\varphi = 0$ , while a pure mode II experiment ( $V = V(t), W \equiv 0$ ) gives

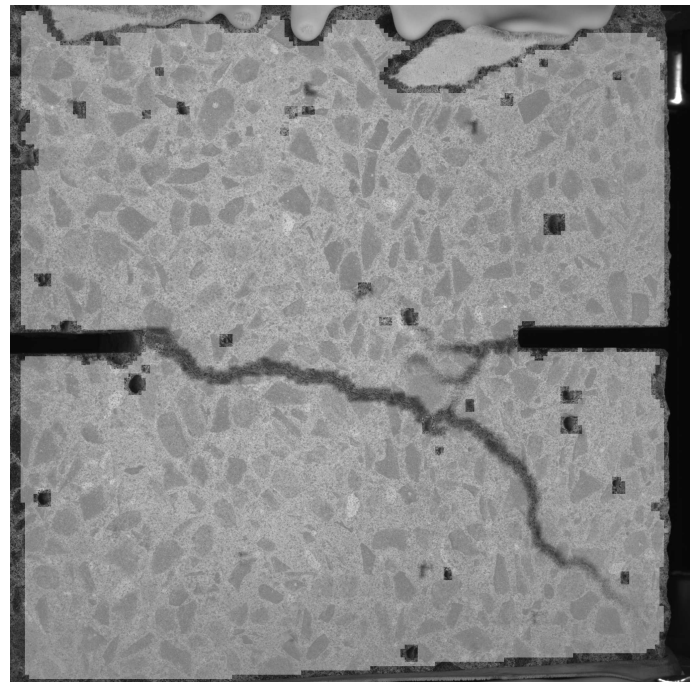


Figure 15: Second crack caused by mixed mode loading,  $\varphi \approx 50^\circ$ .

$\varphi = 90$ . In the mixed-mode experiments,  $\varphi > 40^\circ$  resulted in secondary cracking. The crack pattern for one such experiment is shown in Figures 14 and 15. The figures show that the initial tensile crack closes in the right part of the specimen due to the build-up of a compressive load. Instead, crack opening takes place on the left part of the tensile crack and continues in a new direction down towards the lower platen. The tortuosity of the crack is probably the cause for the observed behavior, as it most likely will be in many cases.

## 6 CONCLUSIONS

Pilot results obtained from a new biaxial testing machine dedicated for the investigation of mixed mode cracking of concrete are presented. The biaxial testing machine has proven to be unforeseen stiff and allows for translationally and rotationally stable fracture mechanical testing of concrete.

The machine has been used in combination with photogrammetric measurement techniques and this tool has shown to be invaluable in mixed mode cracking since it allows for surface measurements revealing crack tortuosity, secondary cracking, non-local cracking, non-uniformity of crack propagation and local measurements of crack widths in the post processing phase.

The pilot experiments have shown that full crack penetration in the uniaxial tension test may not necessarily be achieved until the load has decreased to 50% of the peak load on the unloading branch. This makes it difficult to conduct mixed mode experiments on small crack openings. Also, when mixed mode experiments are conducted, secondary cracking will often occur.

Another result, which may not be surprising, is that the crack in this study always initiates in pure Mode I. Mode II crack sliding is not observed for normal openings of the crack below  $w \cong 0.05$  mm, and is only slowly growing in magnitude after this value. This result was obtained from an experiment where crack initiation away from the specimen boundaries was studied and where the remote loading was dominated by shear load.

## 7 ACKNOWLEDGEMENTS

The support from the Villum Kann Rasmussen Foundation for purchase of the Aramis 4M photogrammetric equipment is highly recognized.

This project has also received funding from the Danish Technical Research Council under the Talent Programme, Project No. 26-03-0333. This contribution is also gratefully acknowledged.

## REFERENCES

- Carol, I., C. M. López, and O. Roa (2001). Micromechanical analysis of quasi-brittle materials using fracture-based interface elements. *International Journal for Numerical Methods in Engineering* 52, 193–215.
- Carpinteri, A. and S. Swartz (1991). Mixed-mode crack propagation in concrete. In S. Shah and A. Carpinteri (Eds.), *Fracture Mechanics Test Methods for Concrete*, Chapter 2, pp. 129–198. Chapman & Hall.
- Gálvez, J. C., M. Elices, G. V. Guinea, and J. Planas (1998). Mixed mode fracture of concrete under proportional and nonproportional loading. *International Journal of Fracture* 94, 267–284.
- Hassanzadeh, M. (1992). *Behaviour of Fracture Process zones in Concrete Influenced by Simultaneously Applied Normal and Shear Displacements*. Ph.d. thesis, Report TVBM-1010, Lund Institute of Technology.
- Hillerborg, A. (1989). Stability problems in fracture mechanics testing. In *Fracture of Concrete and Rock: Recent Developments*, pp. 369–378. Elsevier Applied Science.
- Hillerborg, A., M. Modéer, and P. E. Petersson (1976). Analysis of crack formation and crack growth in concrete by means of fracture mechanics and finite elements. *Cement Concrete Research* 6, 773–782.
- Hordjik, D. A. (1991). *Local Approach to Fatigue of Concrete*. Ph. D. thesis, Delft University of Technology, The Netherlands.
- Nooru-Muhamed, M. B. (1992). *Mixed Mode Fracture of Concrete: An Experimental Approach*. Ph.d. Thesis, Delft University.
- Petersson, P. E. (1981). *Crack Growth and Development of Fracture Zones in Plain Concrete and Similar Materials*. Report tvbm - 1006, Division of Building Materials, Lund Institute of Technology, Lund, Sweden.
- RILEM (2001). Test and design methods for steel fiber reinforced concrete. recommendations for uniaxial tension test. *Materials and Structures* 34(3–6). Prepared by RILEM-Committee-TDF-162, Chairlady L. Vandewalle.
- THK (2000). Thk general catalog. Catalog No. 300-4E.